2007 IEEE International Conference on
Robotics and Automation
Roma, Italy, 10-14 April 2007

A Novel Actuator for High-Precision Alignment in a Nano-Imprint Multi-Layers-Interconnection Fabrication

Tat Joo Teo[1,2], I-Ming Chen[1], Guilin Yang[2] and Wei Lin[2]

Abstract— **This paper presents a novel flexural-based nano-positioning actuator that has a positioning accuracy of 10 nm (limited by encoder resolution) throughout a range of 3 mm. A new dual-magnet configuration is introduced to enhance this electromagnetically driven actuator in achieving 60 N/Amp in a compact configuration. In addition, a constant and evenly distributed magnetic flux density is obtained throughout 11 mm of air gap. A new mathematical model is presented to accurately predict the behavior of magnetic field within the effective air gap of this configuration. Complete analytical models for this actuator's electromagnetic drive and flexural-bearing support element are presented. Lastly, a prototype of this actuator is developed for validating the established analytical models and verifying the claimed capabilities.**

I. INTRODUCTION

Step-and-Flash Imprint Lithography (SFIL) was first reported in 1999 as an emerging technology in the area of nano-feature fabrications [1]. SFIL is a low-cost and high-volume manufacturing process that delivers sub-100 nm features by printing a template with nano-sized pattern onto a layer of substrate. Unlike the conventional nano-imprint lithography, SFIL allows Multi-Layer-Interconnection (MLI) fabrications, which could mark a new era in electronic chip fabrications for semiconductor industry [2]. However, MLI fabrications in an SFIL process pose new engineering challenges in particular to high-precision alignment. This is because as nano-sized features are being built on top of their preceding layers, misalignments at any layer will generate an accumulative alignment error which may break the connectivity of the circuitries. Currently, it is reported that the alignment systems used to produce a well aligned two layers interconnection impression could only reach sub-microns of accuracy [3]. Clearly, such systems are incompetence of producing features with sub-100 nm in depth and spacing between two sets of imprinted patterns. One major reason for such limitations is the lack of an appropriate actuator to drive these existing alignment systems. Due to varies sub-processes in such a nano-imprint process, the system actuators must have several millimeters of travel to maintain enough distance between the template and the substrate [1]. In addition, they must have nanometers of positioning accuracy that is necessary for producing sub-100 nm of layer thickness. Lastly, these actuators also must provide a continuous imprinting force, which range from 60N to 70N for a typical SFIL process.

[1]School of Mechanical and Aerospace Engineering, Nanyang Technological University, Nanyang Avenue, Singapore tjteo@pmail.ntu.edu.sg

[2]Mechatronics Group, Singapore Institute of Manufacturing Technology, 71 Nanyang Drive, Singapore

Unfortunately, initial studies have shown that the existing actuators have limitations in meeting all those requirements. Currently, Piezoelectric (PZT) actuators that are commonly used for nano-positioning have only several hundred microns of travel [4], [5]. Even with added high-resolution pitch screws to achieve several millimeters of displacements, such PZT-driven actuators have poor repeatability due to backlash and Coulomb frictions [6]. Others that use inchworm driving techniques [7] or impact driving techniques [8] to overcome PZT limitations have low payload capacities and slow response speed. As for electromagnetic actuation, voice-coil linear actuators that offer large displacements only produce small output forces [9]. While solenoid actuation produce inconsistent output forces [10]. Even magnetic leviation, which offer nano-positioning over a large workspace [11], are very sensitive to payloads variation. Consequently, limitations of existing nano-positioning actuators have motivated the development of a novel nano-positioning actuator. It will be used to facilitate the alignment stages in realizing high-precision MLI fabrications in a nano-imprint process. In this paper, an actuator, which comprised mainly a dual-magnet configuration with flexural-supported moving coil, is introduce to meet those requirements. A mathematical model that accurately predicts the magnetic field of this magnetic configuration and a complete analytical model of this actuator are also presented. Lastly, a prototype is developed and experiments are conducted to validate the proposed mathematical and analytical models, and verify its claimed capabilities.

II. A NOVEL NANO-POSITIONING ACTUATOR

A. Overview

The novel nano-positioning actuator, or known as a Flexure-based Electromagnetic Linear Actuator (FELA) [12], [13] is proposed to achieve:

1) A few nanometers of accuracy, i.e. ± 10 nm.
2) Millimeters of displacement, i.e. ± 3 mm.
3) Large and continuous output force, i.e. ≥ 60 N.
4) Fast actuating speed, i.e. ≥ 100 mm/s.

A FELA consists of an Electromagnetic Driving Mechanism (EDM), which forms the main element for driving its actuating body (Fig. 1a). A Lorentz-force technique, which consists of a permanent magnet stator and air-coil actuating body, is employed by this EDM for its linearity between input current and output forces. In addition, its competency of achieving infinite positioning resolution and constant output force through the entire range of travel makes

it a promising approach to drive this FELA. The actuating body is then supported by the flexural bearings (Fig. 1b) to form a complete FELA assembly (Fig. 1c).

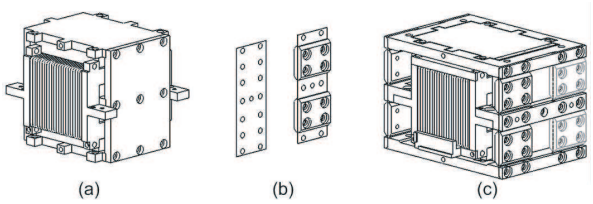

Fig. 1. An (a) EDM with (b) flexural joints to form (c) a FELA.

B. A Dual-Magnet Configuration

A new magnetic configuration is introduced to enhance the capabilities of the EDM [13]. In this work, we name it as a Dual-Magnet (DM) configuration (Fig. 2),which consists of a ferromagnetic stator and two pairs of rare-earth Permanent Magnet (PM), as shown in Fig. 2a. Each pair of PM will be placed in attracting position within the gaps of the ferromagnetic stator and forms an effective air gap between them. The actuating body with conducting coil wound to it is then inserted within the stator to form a complete EDM (Fig. 2b). Unlike a conventional magnetic configuration, a DM configuration offers:

1) Large effective air gap: In a conventional configuration, the magnetic flux density within the air gap varies with respect to the distance from the PM polarized surface. On the other hand, a DM configuration ensures an evenly distributed magnetic flux density throughout the air gap. Thus, magnetic flux density remains constant even at tens of millimeters away from the PM polarized surface.

2) Good force-to-size ratio: To achieve a larger output force, a bigger size PM or longer conducting wire is required in a conventional configuration. Yet any approach will increase the size of an electromechanical actuator. A DM configuration offers 40% higher and evenly distributed magnetic flux density within the effective air gap as compared to the conventional configurations. This allows larger force generation with more compact configuration.

3) Low heat generation: In a SFIL process, a continuous imprint force is required. This continuous force will elevate the coil's heat generation that causes thermal expansion in every material. Such expansions, which can be in nanometric or micrometers, will affect the positioning accuracy of a nano-positioning actuator. A DM configuration allows the EDM to generate large continuous output with small amount of current input that ensures low heat generation and minimize the thermal expansion effect.

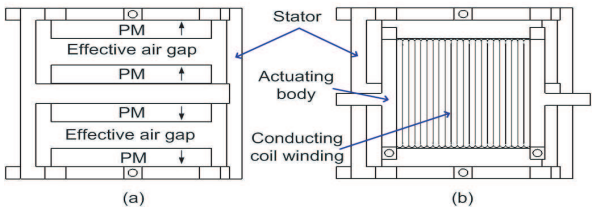

Fig. 2. (a) A symmetrical DM configuration. (b) An EDM

C. Flexural Supporting Bearing

In this FELA, the flexural supporting bearings are employed by its actuating body to provide a smooth, rectilinear and frictionless motion [13]. Known as a Flexural Bearing Mechanism (FBM), it retains the frictionless motions of an electromagnetic driving scheme. The flexural bearings are formed using the shims (Fig. 1b). Most part of the shims will be clamped, leaving the unclamped parts as the free deflection portions that facilitate the displacement of a FBM. The proposed 1-DOF FBM requires a relatively small amount of force to achieve a displacement range of 1.5 mm. In addition, the stiffness of a FBM in non-actuating directions will be a hundred times more than the actuating direction.

III. Current-Force Model

A. Lorentz Force Model

The magnitude of Lorentz force, F, is determined by the magnetic flux density, B, input current, i, and length of coil placed in the magnetic field. In this analysis, coil length is fixed with B varies within the effective air gap. This suggests that F in x-axis (or actuating direction) with the coil wire across in y-axis and B in z-axis can be expressed as,

$$F = i\int_0^{-Coil_y} (-\hat{y}dy) \times (B\hat{z}) \cdot \hat{x} = iNBCoil_y \quad (1)$$

where N is the number of windings and $Coil_y$ is the length of each winding in y-axis. Consequently, (1) suggests that an accurate current-force model will requires a good prediction of the 2D magnetic flux density.

B. Field Potential

For a current-free environment, the magnetic field within the air gap of such a configuration can be reduced to a scalar potential, $\mathbf{\Phi}$, described by Laplace's equation [14], [15].

$$\nabla^2\mathbf{\Phi} = 0 \quad (2)$$

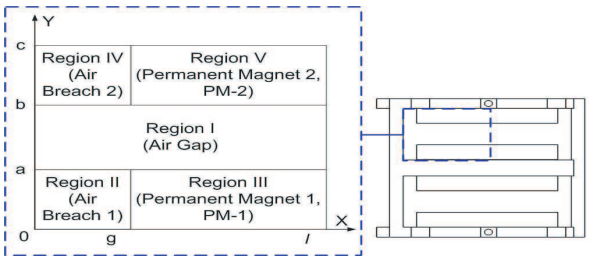

Fig. 3. A 2D geometry of a halved DM configuration.

For 2D field modeling, symmetrical design of a DM configuration is reduced to geometry (Fig. 3) comprised:

1) *Region I*: Air gap of a dual-magnet configuration.
2) *Region II*: Air gap between the PM-1 and stator.
3) *Region III*: PM-1 of a dual-magnet configuration.
4) *Region IV*: Air gap between the PM-2 and stator.
5) *Region V*: PM-2 of a dual-magnet configuration.

Hence, (2) is reduced to 2D Dirichlet boundary-value problem and becomes a linear homogenous partial differentiation equation that can be solved by separation of variables method

with regions describes in Cartesian form. Consequently, the generalized 2D scalar potential for all regions is given as,

$$\Phi_j(x,y) = \sum_{n=1}^{\infty}[S_{j-1}^n cos(k_j^n x) + S_{j-2}^n sin(k_j^n x)] \cdot(S_{j-3}^n e^{k_j^n y} + S_{j-4}^n e^{-k_j^n y}) \quad (3)$$

where j represents the each region (refer to Fig. 3, $j = I, II, III, IV, V$) with coefficients S and k to be determined by the boundary conditions.

C. Boundary Conditions

In this analysis, a superposition of boundary conditions method is proposed to obtain the scalar potential of the effective air gap that is influenced by two magnetic sources, i.e. PM-1 and PM-2. Hence, the scalar potential of the effective air gap will need to be solved separately under the influence of each PM. Consequently, the total scalar potential, $\mathbf{\Phi_I^T}$, of the effective air gap will be the summation of the two scalar potentials, i.e. $\mathbf{\Phi_I^1}$ and $\mathbf{\Phi_I^2}$ .Hence, boundary conditions are made under these assumptions; when analyzing the influence of PM-1, the Regions IV and V are ignored. While analyzing the influence of PM-2, the Regions II and III are ignored. The permeability of the closed-loop stator iron must be infinite. The normal component of the magnetic field strength, $\mathbf{H}$, at the center of the air gap and the PMs is zero. The tangential component of the magnetic field strength at the edge of the vertical closed-loop path is zero. At the interface between effective air gap and PM, the tangential component of magnetic field strength must be continuous. In addition, normal component of magnetic flux density must be also continuous. Lastly, PM is assumed to be ideal and uniformly magnetized throughout. Magnetization, M, within the PM is only orientating normal to the polarization surface. Thus,

$$x = \begin{cases} M\hat{y} & \text{Region III,V} \\ 0 & \text{Region I,II,IV} \end{cases} \quad (4)$$

D. Magnetic Flux Model

Solving (3) using those boundary conditions, yields the scalar potential of air gap influence by PM-1,

$$\Phi_I^1(x,y) = \sum_{n=1}^{\infty} \frac{8Ml(1)^n}{U_I[(2n-1)\pi]^2} sinh[\frac{(2n-1)\pi}{2l}(y-b)] \cdot sin[\frac{(2n-1)\pi}{2l}x] \quad (5)$$

where

$$U_I = sinh[\frac{(2n-1)\pi}{2l}(a-b)]coth[\frac{(2n-1)\pi}{2l}a] - cosh[\frac{(2n-1)\pi}{2l}(a-b)] \quad (6)$$

and scalar potential of air gap influence by PM-2 is given as,

$$\Phi_I^2(x,y) = \sum_{n=1}^{\infty} \frac{8Ml(1)^n}{U_{II}[(2n-1)\pi]^2} sinh[\frac{(2n-1)\pi}{2l}(y-a)] \cdot sin[\frac{(2n-1)\pi}{2l}x] \quad (7)$$

where

$$U_{II} = sinh[\frac{(2n-1)\pi}{2l}(b-a)]coth[\frac{(2n-1)\pi}{2l}(b-c)] - cosh[\frac{(2n-1)\pi}{2l}(b-a)] \quad (8)$$

Consequently, the 2D magnetic flux density within the effective air gap can be re-expressed as,

$$B_I^T(x,y) = -\mu_0[\frac{d\Phi_I^1(x,y)}{dx} + \frac{d\Phi_I^2(x,y)}{dx}] \quad (9)$$

With (1) and (9), the static current-force analytical modeling of the proposed EDM of a FELA is established.

IV. Force-Displacement Model

A. Pseudo-Rigid-Body

A Pseudo-Rigid-Body (PRB) modeling technique [16] is used to describe the behavior of the force-deflection relationship of the flexural joints by modeling them as kinematics rotary joints with torsional springs. The flexural joints of a FBM, which are the unclamped portions of a shim, will be described as a thin cantilever beam. Consequently, the torque, T, generated at the "characteristic pivot" can be expressed as [17],

$$T = (\gamma K_\Theta \frac{EI}{P})\Theta \quad (10)$$

where Θ is the PRB deflection angle of the beam, γ is the "characteristic radius factor", K_Θ is the non-dimensionalized spring constant, EI is the flexural rigidity and P is the length of the beam.

B. Forward Kinematic Analysis

A FBM can be described as a pair of symmetrical linear spring configuration with flexural joints. Each of these linear spring configurations can be represented by a planar four-bar mechanism. Consequently, forward kinematics analysis conducted based on Fig. (4a) suggests that the velocity coefficients are,

$$\begin{Bmatrix} \dot{\theta}_3/\dot{\theta}_2 \\ \dot{\theta}_4/\dot{\theta}_2 \end{Bmatrix} = \begin{Bmatrix} r_2 sin(\theta_4-\theta_2)/r_3 sin(\theta_3-\theta_4) \\ r_2 sin(\theta_3-\theta_2)/r_4 sin(\theta_3-\theta_4) \end{Bmatrix} \quad (11)$$

where θ_2 is primary variable, θ_3 and θ_4 are secondary variables. r_2, r_3, and r_4 represent rigid links.

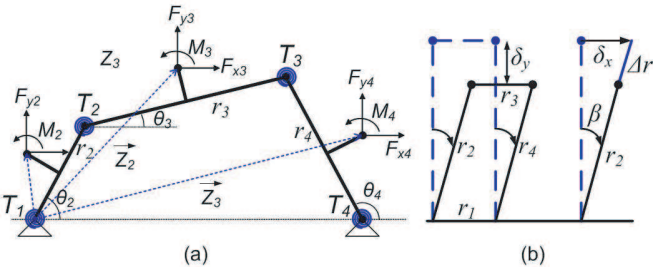

Fig. 4. (a) A schematic representation of a PRB linear spring. (b) A parasitic error at y direction due to motion in x-direction.

C. Force-Deflection Model

The total virtual work done, δW_{SYS}, of a linear spring configuration based on the FBM can be summarized as,

$$\delta W_{SYS} = \sum_{i=1}^{1} \vec{F}_i \cdot \delta \vec{Z}_i + \sum_{i=1}^{4} \vec{T}_i \cdot \delta \vec{\psi}_i \qquad (12)$$

where the first term represents the virtual work done due to a driving force, $\vec{F}$, acting on the rigid link that causes a virtual displacement, $\delta \vec{Z}$, of the rigid link. The second term represents the virtual work done due to all the torsional springs with $\vec{T}_i = -k(\psi)$ and their virtual deflection, $\delta\psi_i = \theta_i - \theta_{i(o)}$, where $\theta_{i(o)}$ is the initial angle of the un-deflected torsional spring. Based on (11), (12) and virtual work principle, the force-displacement relationship of a single flexural joint of the FBM is given as,

$$F_{in\_torsional} = \frac{-4K_T(\theta_2 - \theta_{2o})}{r_2 sin\theta_2} \qquad (13)$$

D. Force-Axial Elongation Model

A single linear spring mechanism gives a parasitic error in Y direction, δ_y, when driven in X direction (Fig. 4b). In this analysis, the axial elongations of the linkages are treated as the linear spring effects using PRB modeling. Consequently, the virtual displacement of this axial elongation, δW_{axial}, can be expressed as,

$$\delta W_{axial} = -\sum_{p=2,4} \{f_k[\frac{r_p}{cos(\beta_p)} - r_p]sin(\beta_p)\}\hat{i} \cdot[-r_p sin\theta_p(\dot{\theta_p})\hat{i} + r_p cos\theta_p(\dot{\theta_p})\hat{j}] \qquad (14)$$

where index, p, indicates the linkage, $\beta_p = 90^o - \theta_p$, and $f_k = \frac{EA}{L}$; E is Young's modulus, A is cross-sectional area of the flexure joints, and L is the length of the flexural joint, Applying virtual work principle, the force-axial elongation relationship of a single flexural joint is given as,

$$F_{in\_axial} = 2f_k[\frac{r_2}{cos(\beta_2)} - r_2]sin(\beta_2) \qquad (15)$$

E. Force-Displacement Model

Consequently, the displacement in x-direction and deflection relationship of a single linear spring mechanism can be expressed as,

$$\delta_x = \gamma L sinh^{-1}(\beta_2) \qquad (16)$$

and force require to achieve a given δ_x can be expressed as,

$$F_{in} = \frac{-16K_T(\theta_2 - \theta_{2o})}{r_2 sin\theta_2} + 8f_k[\frac{r_2}{cos(\beta_2)} - r_2]sin(\beta_2) \qquad (17)$$

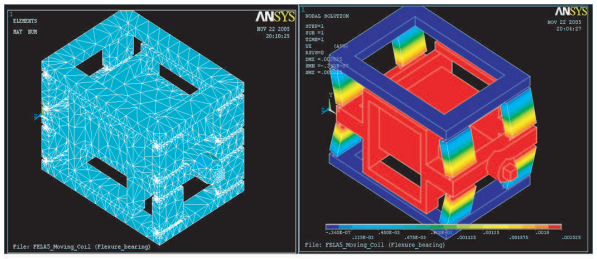

(a) (b)

Fig. 5. A numerical simulation of a FELA in ANSYS 8.1.

TABLE I
FINITE ELEMENT ANALYSIS OF FBM

Type of analysis	Results (Ratio)
Stiffness ratio between x and y directions at +2 mm (x : y) with external force of 11.5N	1 : INF
Stiffness ratio between x and z directions at -2 mm (x : z) with external force of 11.5N	1 : 3.1×10^3
Stiffness ratio between x and y directions at neutral position (x : y) with external force of 11.5N	1 : 1.7×10^3
Stiffness ratio between x and z directions at neutral position (x : z) with external force of 11.5N	1 : 3.1×10^3

V. ANALYSIS

Using ANSYS 8.1, the proposed FBM underwent numerical analyses to determine its stiffness at all non-actuating directions. In those analyses (Fig. 5), stainless steel is selected as the FBM's material. This material is assumed to be linearly elastic with Young's modulus of 190 GPa, Poisson's ratio of 0.31 and SOLID 92 of element type. The numerical analyses conducted through ANSYS 8.1 simulator, have shown that the FBM demonstrated high stiffness in the non-actuating directions at a positive actuating, neutral and negative positions respectively (Table I).

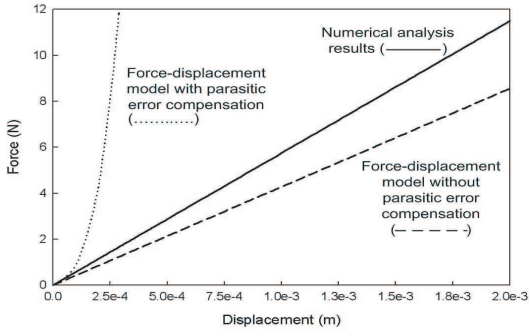

Fig. 6. A static force-displacement analyses of a FBM.

A static force-displacement analyses based on numerical simulator (i.e. ANSYS 8.1) and analytical model (17) is conducted (Fig. 6). The analytical model has shown that the proposed FBM with parasitic error compensation in y-direction demonstrates a non-linear force-displacement behavior. On the other hand, the analytical model returns with a linear force-displacement behavior on the FBM when parasitic error is not compensated.

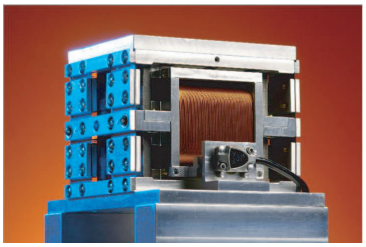

Fig. 7. A complete assembly of a FELA prototype.

VI. PROTOTYPE

A $100 \times 100 \times 70$ (mm) prototype of a FELA is developed (Fig. 7). The flexural joints are form by stainless steel shims and the remaining parts of the FBM are form by aluminum. For the EDM, AWG24 wire (DIA 0.45 mm) is selected based

on an operating temperature of 120^{o}C at 2 Amp. Rare-earth PMs (Type N45M) with residue magnetic flux density of 1.33 Tesla, T, are used to form an effective air gap of 11 mm to optimize the performance of the current EDM design and size.

VII. Experiment and Validation

A. Magnetic distribution of a DM configuration

A LAKESHORE hall-sensor probe and gauss-meter tools are employed to measure the magnetic flux density within the effective air gap. The hall-sensor probe is a single-axis measuring device that is placed within the air gap of a DM configuration. This probe is attached to a X-Y-Z translational manipulator, which runs a pre-programmed measure loop. The gauss-meter is connected to a Personal Computer (PC) to display the amount of magnetic flux density instantaneously in Tesla scale with 0.001 T of noise resolution. From Fig. 8(a), the experimental results have shown that a DM configuration offers a large effective air gap of up to 11 mm with a consistent and evenly distributed magnetic flux density within it. Most importantly, Fig. 8(b) shows that the established analytical model 9 has accurately predicted the magnetic flux behaviour and distribution within the effective air gap up to an accuracy of ± 0.01 T. Consequently, this analytical model will be used for design optimization of a DM configuration in future.

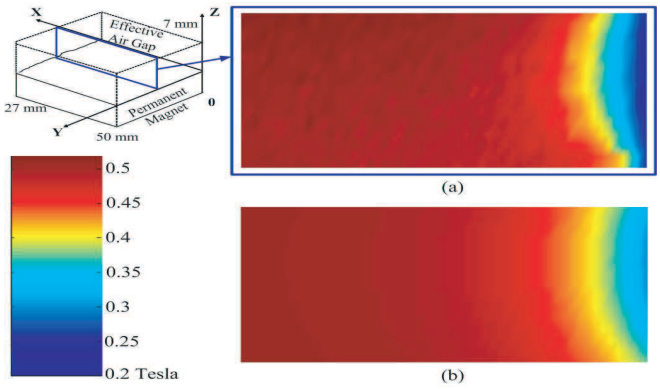

Fig. 8. Magnetic flux density within the effective air gap obtained from (a) experiments and (b) analytical model.

B. Output force of a FELA

A force measurement was performed on the FELA using a THRUST DC linear amplifier and a 6-DOF force/torque sensor from ATI. From Fig. 9, the experimental results have shown that the relationship between the input current and the output force is linear. The FELA generates a 6 N of output force using 0.1 Amp of input current. Due to the low power rating of the linear amplifier, input current is limited to 0.5Amp. With a larger VDC linear amplifier, a FELA will be capable of generating 120 N of output force with 2 Amp of input current based on such a linear relationship. The analytical solution based on the established current-force model and experimental data was plotted in Fig. 9. The difference can be explained by the presence of vector potential due to the existence of current source (or vector potential). As both scalar and vector potentials agree with Hamiltonian principle, vector potential will have a direct affect on the magnetic field. As the current analytical solution is based on a current-free assumption (9), a more comprehensive magnetic field model that includes this vector potential will be introduced in near future.

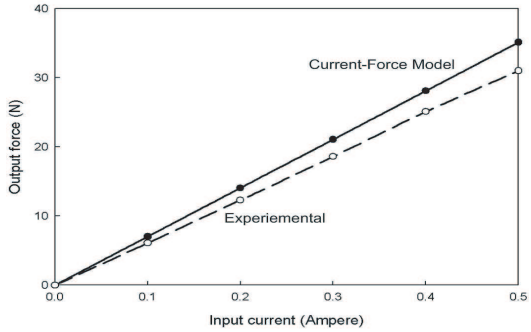

Fig. 9. A input current and output force analysis based on analytical model and experimental results.

C. FELA for High-precision Positioning

A simple PID position control had been implemented on the FELA to validate its positioning accuracy and displacement range. This control system mainly consists of an industrial PC, a NI controller card, a linear amplifier and a MicroE-Systems optical linear encoder (5 nm/count resolution). The control frequency of this system is 1 kHz with 10 kHz PID servo-loop.In this analysis, a set of PID parameters has been used for fine and large positioning tasks. All tasks are done at actuating speed of 100 mm/sec.

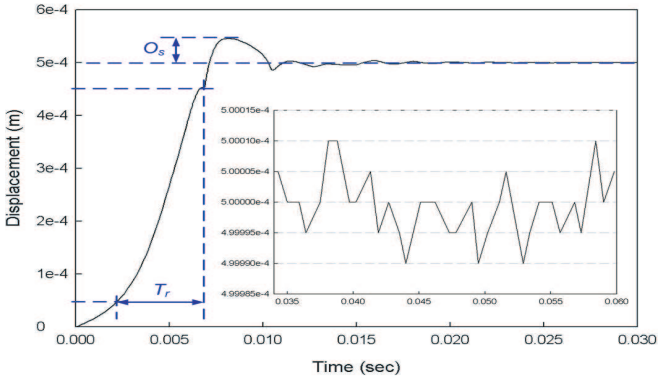

Fig. 10. A step response of FELA from 0 to 0.5 mm.

A step response of the FELA from 0 to 0.5 mm was plotted in Fig. 10. It shows a rise time, T_r, of 3.4 msec and a overshoot, O_s, of 8.4%. It settles after 10 msec and reaches position accuracy of ± 10 nm after 30 msec. Fig. 11 shows a ± 10 nm of positioning accuracy obtain at every 30 nm repetitive step. Lastly, a large displacement positioning is performed on FELA. From Fig. 12, FELA moves from 0 to 1.5 mm and settles at 10 nm after 0.4 sec. At this point of time, the positioning accuracy of the FELA is limited by the current encoder resolution. By referring to Fig. 11, variations with $\pm$ 1 $\sim$ 2 encoder count have suggested that a higher resolution encoder will increase FELA's positioning accuracy.

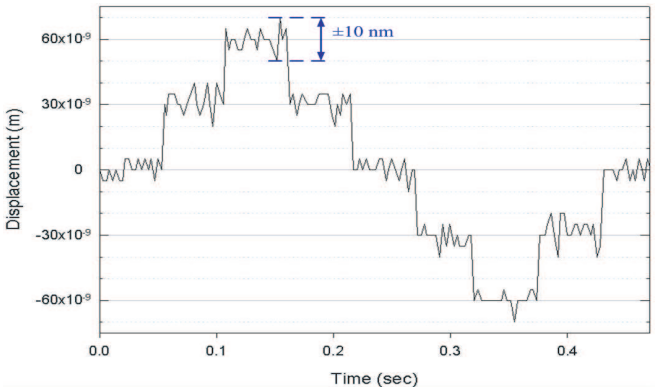

Fig. 11. A 30 nm repetitive step.

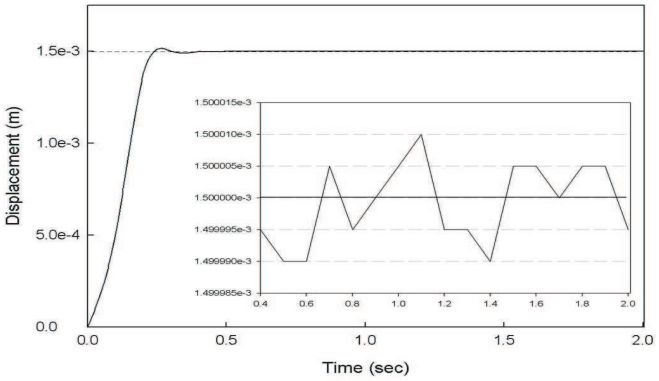

Fig. 12. A large displacement from 0 to 1.5 mm performed by FELA.

VIII. Conclusion

A novel nano-positioning actuator with large displacement and large continuous thrust force has been developed in this work. Known as a FELA, it will be implemented as the actuating systems in a proposed high-precision alignment stage for a nano-imprint machine (Fig. 13). A new DM configuration is introduced as the main element that contributes to a FELA's performances, which are unachievable in conventional electromechanical linear actuators. A new mathematical model has been established to predict the magnetic field of such a new configuration. Its accuracy has also been validated experimentally. A complete analytical model of a FELA's EDM and FEB was also presented. A simple PID position control scheme was implemented to the developed FELA prototype. Results have shown its capability of achieving 10 nm of positioning accuracy (limited to current encoder resolutions) over a displacement of 3 mm. Lastly, the linearity of current-force suggests that a compact-sized FELA is capable of generating 60 N/Amp of continuous thrust force. With those capabilities, this FELA has potential of facilitating the alignment systems to realize high-precision MLI fabrications in a nano-imprint process.

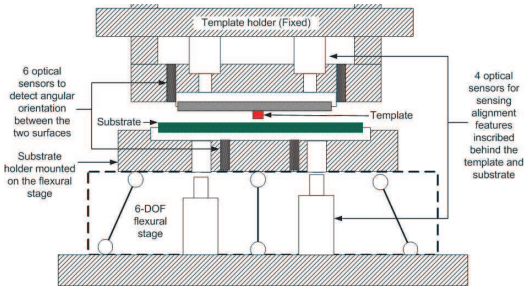

Fig. 13. A proposed 6-DOF machine for MLI fabrication in SFIL.

IX. Acknowledgments

T. J. Teo would like to thank Singapore Institute of Manufacturing Technology, Agency of Science, Technology & Research (A*STAR) for the financial support on his PhD study and this project.

References

[1] M. Colburn, S. C. Johnson, M. D. Stewart, S. Damle, T. C. Bailey, B. Choi, M. Wedlake, T. B. Michaelson, S. V. Sreenivasan, J. G. Ekerdt, and C. G. Willson, "Step and flash imprint lithography: a new approach to high-resolution patterning," *Emerging Lithographic Technologies III*, Santa Clara, CA, USA, 1999, pp. 379-389.

[2] M. Colburn, A. Grot, M. N. Amistoso, B. J. Choi, T. C. Bailey, J. G. Ekerdt, S. V. Sreenivasan, J. Hollenhorst, and C. G. Willson, "Step and flash imprint lithography for sub-100-nm patterning," *Emerging Lithographic Technologies IV*, Santa Clara, CA, USA, 2000, pp 453-457.

[3] B. J. Choi, S. V. Sreenivasan, S. Johnson, M. Colburn, and C. G. Wilson, "Design of orientation stages for step and flash imprint lithography," *Precision Engineering*, vol. 25, pp 192-199, 2001.

[4] C. Woo Sok and K. Youcef-Toumi, "Modeling of an omni-directional high precision friction drive positioning stage," *Proc. of IEEE International Conference on Robotics and Automation*, vol.1, 1998, pp 175-180.

[5] M. Rakotondrabe, Y. Haddab, and P. Lutz, "Step Modelling of a High Precision 2DoF (Linear-Angular) Microsystem," *Proc. of IEEE International Conference on Robotics and Automation*, 2005, pp 150-156.

[6] New-Focus, "Pico Motor," New Focus, 2005.

[7] EXFO-Burleigh, "Piezoelectric Inchworm actuator," EXFO Burleigh, 2005.

[8] Y. Yamagata and T. Higuchi, "A micropositioning device for precision automatic assembly using impact force of piezoelectric elements," *Proc. of IEEE International Conference on Robotics and Automation*, vol.1, 1995, pp 666-671.

[9] B. Sprenger, O. Binzel, and R. Siegwart, "Control of A High Performance 3 DOF Linear Direct Drive Operating With Submicron Precision," *4th International Conference on Motion and Vibration Control*, MOVIC '98, Zurich, 1998, pp 1145 - 1150.

[10] K.-S. Chen, D. L. Trumper, and S. T. Smith, "Design and control for an electromagnetically driven X-Y-[theta] stage," *Precision Engineering*, vol. 26, 2002, pp 355-369.

[11] S. Verma, W.-j. Kim, and J. Gu, "Six-axis nanopositioning device with precision magnetic levitation technology," *IEEE/ASME Trans. on Mechatronics*, vol. 9, 2004, pp 384-391.

[12] G. Yang and T. J. Teo, "A Flexure-Based Electromagnetic Linear Actuator," in *Intellectual Property Office of Singapore: A-STAR: Exploit Technologies Pte Ltd*, 2005.

[13] T. J. Teo, I.-M. Chen, G. L. Yang, and W. Lin, "A Flexure-Based Electromagnetic Linear Actuator for Nano-Positioning," *RoManSy 16*, Warsaw, Poland, 2006, pp 371-378.

[14] J. C. Maxwell, *A Treatise on Electricity and Magnetism by James Clerk Maxwell* Unabridged 3rd ed. ed: Oxford: Clarendon Press, 1998.

[15] E. P. Furlani, *Permanent Magnet and Electromechanical Devices*, Academic Press, 2001.

[16] L. L. Howell and A. Midha, "A Method for the Design of Compliant mechanisms with Small-Length Flexure Pivots," *ASME Journal of Mechanical Design*, vol. 116, 1994, pp 280 - 290.

[17] L. L. Howell and A. Midha, "Parametric Deflection Approximations for End-Loaded, Large-Deflection Beams in Compliant Mechanisms," *Transaction of the ASME*, vol. 117, March 1995, pp 156 - 165.